Naval Research Laboratory

Washington, DC 20375-5320

NRL/MR/6350--18-9807

On Challenges in Developing a High-Fidelity Model of the Human Head for Traumatic Brain Injury Prediction

Robert Saunders

Mulifunctional Materials Branch

Material Science and Technology Division

Nithyanand Kota

Leidos, Inc.

11951 Freedom Drive

Reston, VA

Amit Bagchi

Mulifunctional Materials Branch

Material Science and Technology Division

Siddiq Qidwai

National Science Foundation

2415 Eisenhower Avenue

Alexandria, VA

October 3, 2018

REPORT DOCUMENTATION PAGE

Form Approved
OMB No. 0704-0188

1. REPORT DATE *(DD-MM-YYYY)*	**2. REPORT TYPE**	**3. DATES COVERED** *(From - To)*
03-10-2018	Memorandum Report	October 2016 - September 2017

4. TITLE AND SUBTITLE

On Challenges in Developing a High-Fidelity Model of the Human Head for Traumatic Brain Injury Prediction

5a. CONTRACT NUMBER

5b. GRANT NUMBER

5c. PROGRAM ELEMENT NUMBER
61153N

6. AUTHOR(S)

Robert Saunders, Nithyanand Kota*, Amit Bagchi and Siddiq Qidwai**

5d. PROJECT NUMBER

5e. TASK NUMBER

5f. WORK UNIT NUMBER
63-1B44-A-8-5

7. PERFORMING ORGANIZATION NAME(S) AND ADDRESS(ES)

Naval Research Laboratory
4555 Overlook Ave., S.W.
Washington, DC 20375

8. PERFORMING ORGANIZATION REPORT NUMBER

NRL/MR/6350--18-9807

9. SPONSORING / MONITORING AGENCY NAME(S) AND ADDRESS(ES)

1. Office of Naval Research through the NRL Basic Research Program
2. Department of Defense High Performance Computing Modernization Program (HPCMP) at AFRL, Major Shared Resource Center (MSRC), Project 416, Subproject 572
3. Office of Naval Research, under contract number N001415WX00531

10. SPONSOR / MONITOR'S ACRONYM(S)

11. SPONSOR / MONITOR'S REPORT NUMBER(S)

12. DISTRIBUTION / AVAILABILITY STATEMENT

DISTRIBUTION STATEMENT A: Approved for public release; distribution is unlimited.

13. SUPPLEMENTARY NOTES

*Leidos, Inc. 11951 Freedom Drive, Reston, VA 20190
**National Science Foundation, 2415 Eisenhower Avenue, Alexandria, VA 22314

14. ABSTRACT

This report elucidates current challenges in development of predictive high-fidelity human head models for traumatic brain injury. Various developmental stages of the NRL high-fidelity head model, are used to describe the challenges encountered and how they can be overcome. Semi-automatic segmentation procedures, meshing to balance fidelity and cost of computation, realistic boundary and contact conditions, accurate component constitutive models based on published data, and validation with experimental output from PMHS subjects are explained. The elucidation of specific and overarching challenges are expected to enable appreciation and creation of better computational models.

15. SUBJECT TERMS

human, validation, simulation, traumatic brain injury,
finite element, biomechanics, high-fidelity, TBI, FEA, modeling

16. SECURITY CLASSIFICATION OF:			**17. LIMITATION OF ABSTRACT**	**18. NUMBER OF PAGES**	**19a. NAME OF RESPONSIBLE PERSON**
					Dr. Amit Bagchi
a. REPORT	**b. ABSTRACT**	**c. THIS PAGE**	Unclassified Unlimited	47	**19b. TELEPHONE NUMBER** *(include area code)*
Unclassified Unlimited	Unclassified Unlimited	Unclassified Unlimited			(202) 767-3094

Standard Form 298 (Rev. 8-98)
Prescribed by ANSI Std. Z39.18

This page intentionally left blank.

Table of Contents

This page intentionally left blank.

Executive Summary

The objective of this report is to elucidate the current challenges associated with the development of predictive high-fidelity human head models for traumatic brain injury (TBI). The focus on high fidelity is based on the premise that precise predictive capability requires the incorporation of the structural complexity of the head into the computational model. Similarly, the need to develop predictive TBI models is self-evident considering available casualty data from recreational sports to automotive industry to war zones. While there have been several noteworthy efforts in recent years on the development of human head models for TBI with ever improving fidelity, they have been almost exclusively discussed in the context of their intended application. Here, the various developmental stages of a head model, the NRL high-fidelity head model (NRL-HFHM), are used to describe the challenges encountered and how they can be overcome. Thus, semi-automatic segmentation procedures, meshing to balance fidelity and cost of computation, realistic boundary and contact conditions, accurate component constitutive models based on published data, and validation with experimental output from PMHS subjects are explained. The specific and overarching challenges associated with these assumptions and analyses are discussed in the context of the experimental work. Additionally, the model output data from validation simulations have been analyzed to assess the prospects of TBI in the simulated subject based on published injury metrics as well as compare the apparent similarities and differences. The developmental narrative used here will have universal appeal across the computational biomechanics discipline because of the similarity of processes and will enable appreciation and creation of better computational models.

This page intentionally left blank.

Introduction

Improved understanding of traumatic brain injury (TBI) arising from various threats, including blunt impact or interaction of blast waves with the head, can be achieved by accurate computational modeling of the phenomenon. Development of these predictive computational models requires a high-fidelity geometric model combined with appropriate descriptions of the constituent materials as well as experimental data for validation. To obtain the anatomical features of the human head accurately, digital images, such as magnetic resonance imaging (MRI) and computed tomography (CT) data, must be segmented manually to identify all the features in the head. Next, experimental stress-strain data on biological tissues must be compiled and analyzed to calibrate material models. The calibration process requires the ability to capture effects such as large strain elasticity, deformation rate, directional dependence, and hysteresis. Once an appropriate description of the geometry and material behavior is constructed, the model needs to be validated. Validation is most commonly done using experimental data from post-mortem human subjects (PMHS) subjected to blunt impact or similar loading profiles. Such validations are often partial due to the inherent deficiency of the PMHS in representing a living human brain. Age of the PMHS compared to that of the human subject used for the computational model and incomplete information on experimental conditions for many of such experiments are also causes for the incompleteness of many validation attempts. In spite of these limitations, use of PMHS provides a good approximation for testing a human brain with its complex biological connectivity to the rest of the body and its organs.

Computational modeling of the human head has evolved considerably over the past few decades with advances in imaging and computational segmentation techniques. Some of the earliest computational models of the human head for blast and blunt impact injury described the head as a simplified geometric structure with a series of nested spheroidal and ellipsoidal structures (*e.g.,* [1]), while others represented the head with coarse representations of anatomical features (*e.g.,* [2]). Due to a lack of image processing techniques, all models developed at this early stage lacked facial features and complex topological features inside the head. In addition, the constitutive models were also simple, being linear elastic, viscoelastic, or completely rigid (*e.g.,* [3]). These head models were also limited by computing resources and consequently used a coarse finite element mesh comprising fewer than 1000 elements.

In the next phase, continued advances in image processing and computing power allowed for the generation of models that resembled the human head more closely, meshed with greater than 1000 elements [4–6]. This was aided greatly by the National Institutes of Health (NIH), which introduced an open source image processing software, ImageJ [7], and a publicly available set of high resolution CT and MRI scans of

Manuscript approved October 3, 2018.

the human head and body, known as the Visible Human Project [8]. The combination of ImageJ and the Visible Human Project led to the creation of the highest resolution models of the era [9,10], with component features such as the skull, cerebrum, cerebellum, falx, tentorium, spinal cord, and various other tissues and bones. The increase in geometric fidelity was accompanied by an increase in fidelity of the constitutive models. Large strain elasticity was simulated more accurately using hyperelastic constitutive models and incompressible materials were numerically described with pressure-displacement relationships rather than assumed rigid.

Model fidelity has continued to increase as time has progressed and numerous models of the head have been created more recently with the intent to simulate traumatic brain injury. The National Highway Safety Authority has developed the simulated injury monitor (SIMon) head model to simulate brain injury due to traffic collisions [11–13]. Wayne State University has developed the Wayne State University Brain Injury Model (WSUBIM) to simulate impacts known to cause mild traumatic brain injury in sports [4,14–16]. Researchers at the Defense and Veterans Brain Injury Center (DVBIC) and Massachusetts Institute of Technology (MIT) have developed the DVBIC-MIT full head model to simulate blast loads using a Lagrangian approach [17], while researchers at Sandia National Laboratories and the University of New Mexico have developed a similar model to simulate blast events using an Eulerian approach [18]. This list is not meant to be exhaustive, as many other models of varying levels of geometric fidelity have been developed for a number of other purposes. For instance, El Sayed *et al.* [19] have developed a brain model that uses a constitutive model, which combines finite viscoelasticity and finite elastoplasticity with decoupled volumetric and deviatoric responses. This model does not use the highest level of geometric fidelity but is able to predict brain injury using damage parameters obtained from the constitutive model response [20]. Another example is the multiscale modeling work of Cloots *et al.* [21], where a macroscale head model is used to predict loads that could be applied to a microscale tissue model with the aim of accurately predicting axonal strain.

All the models to date have continuously and incrementally contributed to head modeling utilizing the latest tools available at the time. However, the development of a human head model, or any biofidelic computational model, is still fraught with issues from geometry creation to material representation to validation against experiments. Thus, in this work, we seek to highlight the core issues that arise during the creation and validation of a high-fidelity human head model and in the process provide guidance to future model developers and experimentalists.

We seek to do this by developing a high-fidelity human head model and using it for simulations following the investigative style laid out by Erdemir *et al.* [22] and commenting on specific challenges throughout the process. Thus, we first focus on the model identification and structure, which are followed by the simulation structure. Then, the verification of the software and comparison against four common experiments used for validation, and the associated issues in validating a computational

model against these experiments are described. Simultaneous analysis on each of the four experiments is also conducted to evaluate the type and extent of injury, if any, which would have occurred in an *in-vivo* subject. Lastly, the main conclusions emerging from this effort are provided as a commentary on the way forward.

Model & Simulation Details

Model Identification

The computational model developed in this work is a high-fidelity human head and neck model for the simulation of high strain rate effects of blunt and blast loadings. The subject of this head model is a 25-year-old Caucasian male with a height of 1.8 m and a weight of 81 kg. This subject approximately represents a U.S. 50^{th} percentile male [23]. The high-fidelity head model, henceforth referred to as the Naval Research Laboratory high-fidelity head model (NRL-HFHM), features all of the major and minor components that can be differentiated from high-resolution medical images. Emphasis is placed on the geometry and features of the intracranial cavity i.e. the brain-cerebrospinal fluid (CSF) complex. The novelty of this model is the resolution at which the head features are incorporated to capture phenomena such as wave reflections due to impedance mismatch between components and multiplicative focusing of waves due to geometric features. The drawback to this approach is the large number of elements needed to resolve this geometry and the corresponding number of degrees of freedom needed to be solved for at each time step in the finite element (FE) scheme.

Blast and blunt impacts happen over the range of milliseconds and are induced either by a strong pressure wave or a direct transfer of momentum from an impact to the subject. These events result in high strain rates that can potentially cause injury in the human brain. The exact multiscale mechanisms of these brain injuries are still being debated (*e.g.,* see [24]), but the onset of injuries at the macroscale are nonetheless described through critical values of kinetic and kinematic measures, such as acceleration, stress, strain, and pressure [12,15,25–30]. Many measures at the meso- or micro- scales, such as axonal strain [31] and alterations in electro-biochemical response of the brain [32], have also been suggested recently as representative of brain injury.

Model Structure

NRL-HFHM was developed in collaboration with Simpleware, Inc. (Synopsys®, Mountain View, USA) using magnetic resonance imaging (MRI) scans obtained in vivo at the Exeter MR Centre, UK. The T1 weighted scan of the subject was performed at approximately a 1 mm isotropic resolution, with the dimensions of the final scan volume being 530 mm by 530 mm by 312 mm. The approximate mass of scanned volume is estimated to be 6.5 kg. The MRI images were semi-automatically segmented using the ScanIP software

by Simpleware, Inc. based on gray scale data associated with the images. For more information on the segmentation and mesh generation process, the interested reader is directed to [33,34]. Table 1 lists the anatomical structures included in NRL-HFHM.

Segmentation

During segmentation, many challenges arose. The first was the insufficient resolution of gray scale data and a lack of clarity that are natural to MRI scan techniques. In regions where clarity or resolution was lacking the component segmentation was accomplished either by manual manipulation or supplemented by a computer aided design (CAD) representation of the components desired. Manual segmentation was required in regions such as the brain that consist of two similar materials, i.e. the white and grey matter, and CSF and ventricles, which can be differentiated by visual inspection but is hard to automate. Even visual inspection was not sufficient, however, for component features with length scales at less than the MRI resolution, *e.g.,* the meningeal membranes and associated topologies. Therefore, while dura mater was universally accounted for through manual intervention, the pia mater, the arachnoid, and the sub-arachnoid complex with arachnoid trabeculae and granulations were not explicitly incorporated due to the dual challenges of complexity and paucity of information. Pia mater was only included around the optic nerve where it acts as a sheath; however, the CSF in the subarachnoid complex is represented. Due to insufficient resolution of MRI scans, CAD models of the facial and neck musculature were taken from a library of STL (standard tessellation language) files and modified as needed for the current subject [34].

To partially surmount the use of CAD models, one could utilize a combination of MRI and CT images of the subject. The addition of CT images to the MRI images allows high-resolution visualization of both hard and soft materials. However, CT and MRI scans require two different machines and introduce the challenge of exact patient positioning so that the scans will overlay exactly or even finding the same patient available for both scans. Future technologies could allow for simultaneous imaging [35,36] and eliminate this concern. Although, the difficulties in the visualization of soft materials with similar gray scale contrast will not necessarily be relieved by this procedure.

Mesh Generation

The geometric information of the head model in the multi-part segmented dataset was meshed using multi-part surface decimation algorithm followed by a mixed Delaunay Advancing front approach [37]. NRL-HFHM consists of both solid sections and thin membranous regions represented by shell sections. Shell sections are identified in Table 1. The resulting finite element model consists of approximately 4.6 million tetrahedral and triangular shell elements with exact element counts shown in Table 2. Initially a mixed hexahedral-tetrahedral mesh was implemented in the model but it was

determined that an unstructured fully tetrahedral mesh was able to capture the geometric details of the head with a significantly reduced number of elements [34]. (While completely hexahedral meshes may be more desirable due to numerical accuracy, computational cost is overly prohibitive in achieving the refinement under consideration here.) The average element size, or in other words, the average element density was determined based on the results of a computational convergence study described later.

Initially, the fully tetrahedral mesh was composed of linear elements to reduce computational cost but an overly stiff behavior associated with volumetric locking was noticed in nearly incompressible regions such as the brain. To surmount volumetric locking, quadratic elements are placed in near incompressible regions (for implementation in Abaqus/Explicit [38]). Note that in some FE solvers, a linear tetrahedral formulation is available that uses an elemental volume-averaged pressure to prevent locking [39] while maintaining the low computational cost of a linear element. Two choices are generally available when implementing quadratic elements in a model, a true quadratic fifteen-node tetrahedron [40] and a serendipity ten-node tetrahedron [41]. The serendipity tetrahedron has been chosen for NRL-HFHM based on availability in Abaqus. The serendipity tetrahedron has 4 integration points with ten nodes and an elemental volume-averaged pressure. This allows the element to avoid volumetric locking while maintaining the ability to represent curved geometry. The ten-node tetrahedron, thus, represents a compromise between the hybrid linear element and the computationally expensive fifteen-node quadratic element.

As Table 2 presents, NRL-HFHM consists of a mesh with modified ten-node quadratic tetrahedral elements (Abaqus designation C3D10M), linear four-node tetrahedral elements (Abaqus designation C3D4), and linear three-node triangular shell elements (Abaqus designation S3R). The ten-node elements are used in nearly incompressible regions (brain white matter and grey matter, spinal cord, CSF, ventricles, bridging veins and blood vessels, optic nerves, and eyes) with four-node elements filling the remainder of the space. The regions associated with each element type are shown in Figure 1. This method was implemented so that computational time could be reduced and volumetric locking eliminated. The drawback of using a mixed order model is the discontinuity introduced at the interfaces between element types, which must be resolved by using appropriate contact conditions.

In the setting shown in Figure 1, the dura mater membrane shell elements separate the quadratic element-based CSF and the linear element-based skull. The interfaces between these regions consist of nodes shared between a C3D10M element, an S3R element, and a C3D4 element. The nodes at these interfaces are duplicated such that there are three nodes occupying the same location, each assigned to a different element connectivity matrix. This serves a dual purpose: First, it resolves the discontinuity introduced by different order elements at an interface. Second, it allows studying the effect of CSF-dura mater-skull contact conditions on brain injury prediction,

which is a highly debated subject due to conflicting results from various studies. Some researchers note that results are relatively insensitive to the contact conditions [16,42] where others have noted substantial differences [43,44]. However, none of these studies consider the actual morphological and kinematic conditions at the brain-skull interface—the brain is connected to the skull through various vascular, neural or membranous connections as well as the brain stem—and within the outer meningeal membranes. In [45], the brain-skull complex is quite intuitively identified as a mass suspended by springs and an elastic element in a rigid container based on *in vivo* MRI observations. Additionally, there are open questions as to how high-rate impact waves can transduce through the meningeal layers because of the structural complexity of the pia-arachnoid complex filled with CSF and arachnoid-dura interface, where a large network of arachnoid trabeculae link the arachnoid mater to the pia mater and arachnoid granulations form wedge-like formations that protrude from the arachnoid mater into the dura mater, respectively [46,47]. Thus, idealized tied and sliding boundary conditions may be oversimplifying the complexity. On the other hand, until more morphological and kinematic clarity is revealed along the lines of observations made in [46,48,49] and, more recently, [47], one is compelled to simplify.

Therefore, for the case of this report only, all C3D4 (dark color regions in Figure 1a) to S3R (regions where light and dark colors in Figure 1a meet) interfaces are tied to one another while all S3R to C3D10M (light regions in Figure 1a) interfaces are set as sliding unless otherwise noted; *e.g.,* skull-dura interface is tied whereas dura-CSF interface is sliding. Additionally, the interface between the brain (grey matter) and CSF is set as tied unless noted otherwise. (Note that the CSF in these locations is also representative of the solid components of the pia-arachnoid complex.) All of these conditions can be easily modified and future work will quantitatively examine the effects of these conditions.

Constitutive Representation

In addition to an accurate geometric representation, appropriate constitutive representation of components is essential in increasing the computational accuracy of the finite element models. The physical behavior of biological materials under mechanical loading often requires nonlinear, rate dependent constitutive formulations. The process to obtain these constitutive formulations and their required parameters uses a significant amount of experimental data for each component in the model. Unfortunately, current standards and facilities for mechanical testing of biological materials are woefully insufficient, or almost non-existent in the case of higher rate dynamic behavior determination (*e.g.,* in the important mid-scale rates of 100-500 /s). To develop a human head model for studying blunt and blast loads, an ideal material calibration data set would 1) come from a human subject, 2) comprise of full loading-unloading characterization in tension, compression, and shear as well as shear relaxation and creep response, 3) include rate dependence, *i.e.,* quasi-static to ≥500/s

strain rate, 4) account for spatial variations in the tissue, *e.g.,* the fiber direction in muscles, and 5) represent subject to subject and interspecies variations. As expected, a data set that contains all of this information is nearly impossible to obtain or collect presently. Thus, constitutive models must be calibrated in non-unique ways and cannot be expected to be fully representative of the component behavior.

Nevertheless, the first step is choosing a constitutive model, whose functional form will at least reproduce the experimental data available for calibration. The published computational modeling literature mostly provides the calibrated constitutive model for a given component; however, in some instances, the related experimental data may also be given or can be found from a search in the larger biomechanics literature. Thus, the computational modelers must either settle for parameters for an already defined constitutive model or use the provided/published data to calibrate another constitutive model. The first of these two approaches requires only ascertaining that the chosen constitutive model and parameter set are suited for the expected strains and rates. The second approach allows more flexibility in the choice of the constitutive model but requires considerably more effort to obtain a "good" parameter set. In the spirit of best practice, an effort to calibrate a more advanced constitutive model necessitates using a compilation of data sets for the same material from multiple sources to cover directionality, and different strains and strain rates, which in turn, makes calibration more challenging.

Choosing the best constitutive model form to represent a material can sometimes be confounding because a number of different hyperelastic or viscoelastic constitutive models, each with its strengths and weaknesses [50], can represent large-strain elasticity or time-dependent elasticity, respectively. This selection process for the "best suited" constitutive model can be simplified with the aid of software like the embedded tools in Abaqus/CAE and MCalibration [51], which can calibrate a number of different common constitutive models to an array of datasets rapidly. However, these programs may not always be able to capture complex behavior such as the large-strain rate-dependent elasticity exhibited in experimental data. In such cases, a functional form must be developed from the strain energy to represent the material behavior and an optimization routine with appropriate constraints must be implemented, to accurately match the constitutive model to the experimental datasets by searching the parameter space.

For NRL-HFHM, all materials identified as viscoelastic or hyper-viscoelastic in Table 1 were calibrated by choosing an existing functional form or augmenting it and using a corresponding optimization routine. Materials identified as elastic or hyperelastic were calibrated via a combination of Abaqus/CAE and previously defined parameters. For complete information on the constitutive model selection, experimental datasets, calibration method, and obtained parameters, the interested reader is referred to [52]. However, one point of caution merits mention here due to its importance in numerical convergence. The stability of the constitutive model should be

ensured during the optimization process for the expected range of strain and/or strain rates during simulations through an appropriate selection of model parameters. This can be achieved by imposing a suitable constraint on the optimization process, *e.g.,* the Drucker stability criterion [53,54]. In addition to the uniaxial data calibration, some materials, such as skull, vertebra, and bridging veins, required a directionally dependent constitutive model. For the bridging veins, a primary axis was assigned along the longitudinal axis of the vein (e.g. the direction of blood flow through the vein) and in-plane isotropy (orthogonal to the longitudinal axis) was assumed. The cervical vertebrae were taken to be transversely isotropic and assigned an orientation that had the stiffest component following the spine longitudinal direction. The skull was partitioned into 1000 regions with similar outward normal as shown in Figure 2 and the normal at the center of each region was assigned the out of plane direction for that particular region. Two additional mutually perpendicular directions to the out of plane direction were chosen as the in-plane axes representing the orientation of the region.

Simulation Structure

NRL-HFHM finite element types, as mentioned before, have been chosen from the library in Abaqus/Explicit for the purposes of this report. This does not preclude its implementation in another FE solver, be it one based on an Eulerian or Lagrangian framework. For implementation in an alternate solver, the mesh structure, constitutive models, and specific loading type may need to be updated to be compatible with that solver. NRL-HFHM has been tested or verified to run on Abaqus/6.11 through Abaqus/2017 using the explicit dynamic solver method with default bulk viscosity parameters. For this work, NRL-HFHM was simulated on an SGI Ice-X system using 216 Intel E5-2699v3 cores with a speed of 2.3 GHz and an available memory of 756 GB. Due to some small elements in the model making up a tiny fraction of the volume, the calculated stable time increment by the explicit solver was calculated initially as 1.24 ns. Variable mass scaling was implemented to introduce artificial mass to the smallest elements in the model and thus increase the minimum time increment. For most simulations, 0.1 μs minimum time increment was used. This allowed completing a 30 ms simulation on 216 CPUs in less than 24 hours with a change in total model mass of 1.12%, approximately 75 g. This was deemed incapable of significantly affecting the model inertial response.

Upon completion of the simulation, a Python script was used to process the analysis results. This script used mechanical threshold inputs (Table 3) to determine if an element in the brain had undergone a certain threshold pressure, shear stress, or shear strain. These thresholds were taken from published literature as mechanical predictors that were likely to cause traumatic brain injury; the accuracy or validity of these thresholds is not being considered here and they are merely used for illustrative purposes. It should be noted that while all the criteria were applied in the post processing, many were not triggered and thus could be ignored. In other cases, criteria

based on the same variable but with multiple thresholds were activated, but presentation of the lower criteria did not serve any benefit. For example, when the 235 kPa pressure criterion is satisfied for an element, it may not be necessary to discuss the lower 173 kPa criterion, even though the injured volume for the lower threshold may be of concern in certain instances. The outputs of the Python script indicated which elements had met or exceeded the selected injury threshold as a function of time. This information can be used to demonstrate both possible spatial injury patterns and potential temporal injury volume. The script is currently limited to the primary brain tissues (cerebrum, cerebellum, brain stem), but can be easily extended to other head components assuming injury criteria existed for the components.

Verification & Validation

Verification and validation of a computational model are essential to demonstrate that the model solves the underlying systems of equations correctly and that the expected physical result is produced [55,56]. Most commercial finite element codes, such as Abaqus, are pre-verified in their computational framework—from the operative field equations and implemented constitutive models to the smallest numerical scheme—and thus verification is reduced to ensuring that the necessary verifications procedures have been conducted via the software documentation and that the finite element model under consideration is correctly developed. The later verification typically involves ascertaining element types and quality, and mesh size convergence. (It is assumed that the constitutive models are representative of the material component behavior consequent of the careful calibration scheme.) In large-scale high-fidelity models, the cost (i.e. mesh generation time, model definition time, and computational resources) precludes mesh convergence or sensitivity studies to be exhaustively investigated despite the desirability. Similarly, it is not always possible to maintain element quality universally at all stages of a simulation involving sharp fronts, such as that of a stress wave. In the case of NRL-HFHM, instead of a formal mesh convergence study on the full 3D model, a similar study was carried out for several thick sagittal slices of the head sectioned off the model and, based on it, an appropriate element size (~1 mm critical length) and element types (Abaqus designations: C3D10M, C3D4, S3R) were determined to be acceptable. In addition, it was confirmed for all simulations presented herein that the element quality degradation, if any, was insignificant.

The challenges associated with the validation of a high-fidelity human head model are arguably the primary focus in the development of the model. To elucidate this point, we limit our focus to four experimental works that are most commonly used to validate computational human head models [57], namely, the works of Nahum et al. [58], Trosseille et al. [59], Hardy et al. [60,61], and Yoganandan et al. [62]. All four studies simulate blunt impact on unprotected post-mortem human subjects (PMHS). Three universal challenges can be noted in achieving validation with the data contained

in them. The first is the post-mortem state of the tissue on mechanical properties, which has been suggested to have a drastic effect on tissue mechanical behavior [63]. The second challenge identified is the differences in the *in-silico* head model and the PMHS heads due to dissimilarities in age, sex, and weight, which are all known to affect impact response [64–66]. Finally, we note that all four studies are based on low-rate blunt impact, akin to an automobile accident, which limits their scope for simulation of events that occur at a much faster rate, *e.g.,* blast and ballistic impacts. Now, we look at each study individually and point out specific challenges in their feasibility for validation of a human head model.

Study 1. Nahum et al. [58]

Experiment Setup

The experiment involved a frontal blow on the instrumented head of a seated, stationary cadaver using a padded impactor (Experiment #37) as shown in Figure 3. Special care was taken by Nahum and his team to ensure the static fluid pressurization of the cranial vascular network and cerebral spinal fluid space was maintained at *in-vivo* levels, thus minimizing the effect of post-mortem state. The impact force was measured along with the intracranial subdural pressures in the cadaver head.

Particular Challenges

While original papers by Nahum *et al.* provide a comprehensive description of biological aspects of PMHS study, a few critical aspects essential for comparing against numerical simulations are absent. The first aspect missing for comparison is a sufficient description of the experiment describing the details of the impactor on the PMHS. While the mass of the impactor is given, no information is provided on the type and properties of the padding materials used to modify the impact duration as well as the exact location and area of impact. To circumvent this, simulations have been performed by applying the measured force on the best-judged region of impact as shown in Figure 3b.

Secondly, the locations of subdural pressure sensors are provided from a physiological perspective in the original paper rather than a relative coordinate system, which allows possible measurement location deviations. The pressure sensors were reported to be mounted inside the dura mater flush with the inner surface of the skull, thus the measured pressure is on the surface of the subdural layer or arachnoid encompassing the CSF. This location of a pressure sensor is not ideal for three reasons: i) it does not provide the pressure in the brain, which is a severe limitation from the perspective of brain modeling; ii) it may not capture the actual pressure experienced on the surface if a separation occurs between the sensor face and the tissue; and iii) the impedance mismatches between the dura mater, pressure sensor, and skull can change the dynamics of wave propagation significantly. Based on the descriptions in the paper, the approximate sensor locations are shown in Figure 4. At each sensor location, the

simulated peak pressure was obtained by averaging over a volume in the CSF equivalent to the size of the pressure transducer used in the experiment, which brings in further non-uniqueness in the analysis process. The volume chosen was in the shape of a cylinder with a radius of 2 mm and a depth into the CSF of 1 mm. The depth into the CSF was chosen to account for possible small sensor placement errors inherent to the instrumentation process.

As stated previously, the *in-silico* head model represents a 25-year-old male but the PMHS used in the experiment represents a different subject. In this case (Experiment #37), the body of a 42-year-old male with a comparable head size was used. The breadth (maximum above ears) was 14.5 cm for the PMHS and 15.6 cm for NRL-HFHM. It should also be noted that the PMHS was a full-body subject where NRL-HFHM is a head and neck model only, thus suggesting different boundary conditions in the experiments and the simulation. Jazi *et al.* [67] concluded that the inclusion of a body was not equivalent to free or fixed neck conditions but rather somewhere in between the two. In the current comparison, both fixed and free boundary conditions are applied to the neck and the corresponding results are analyzed.

Comparison & Analysis

The comparison between the simulated and experimental pressures in the frontal, parietal, occipital, and posterior fossa regions are shown in Figure 5 for both free and fixed neck boundary conditions as well as a case with the brain and CSF interface set to sliding rather than tied. (Note: The simulated data is not smoothed.) For the frontal and parietal regions, the results of the simulation agree well with the experiment at early times but start to disagree at later times. For the posterior fossa region, the trends seen in the experiment are predicted by the simulation but the magnitudes differ. For the occipital region, the experimental data is asymmetric despite symmetric positioning of the sensor and application of load. This discrepancy cannot be explained without additional information. The simulation results again appears to follow trends of the experiment data but without agreement in magnitude of the prediction. This disagreement could possibly be due to the separation of the pressure senor and tissue in the experiment. The results of varying boundary conditions agree well with the results of Jazi *et al.* where early times in the results show no significant differences in response but at later times the results begin to diverge. The effect of the contact condition between the brain and CSF shows a dramatic effect on the results of the simulation where negative pressures are present, *i.e.,* the occipital and posterior regions in Nahum et al's experiment. By disconnecting the brain and CSF, it was hypothesized that negative pressure would not be predicted at the sensor location. This is seen for the occipital region but not in the posterior region. This behavior requires further analysis draw conclusions, which is beyond the scope of this work; however, one may want to consider the contact between the falx and the tentorium with the brain regarding this matter.

To extend the results of Nahum *et al.*'s study, we apply the injury prediction thresholds of Table 3 to the simulation results. In doing this, two of the fifteen predictors suggest occurrence of non-negligible (>1% brain volume) injury: 173 kPa pressure and 5% principal strain criteria. The volumetric percentage of the brain exceeding these thresholds for non-negligible injury is plotted against simulation time in Figure 6. Note that the simulation time of 0 ms shown in Figure 6 corresponds to approximately 2.5 ms in the experimental data shown by Nahum *et al.* shown in Figure 5. In examining Figure 6, a few things can be noted. First, injury due to high pressure occurs very early in the impact and does not increase after the initial rise. Next, we note that the pressure-based injury prediction is unchanged regardless of the boundary conditions indicating that such injury is purely a function of input load and the inertia has no effect. As expected, this is not the case for the strain based injury criteria; the boundary conditions appear to have a significant effect on the volumetric percentage of the injured brain based on the 5% principal strain criteria. It is interesting to note that even though the injured brain volumetric percentages are very different for both pressure and strain based criteria, the evolution of the injury patterns is similar. In Figures 6(a) and 6(b), a small rise is seen in both results at approximately 2 ms followed by a second, significant rise at around 5.5 ms. The second rise is the only place where a difference in the boundary conditions can be noticed. This is due to the head starting to exhibit rigid body motion.

Representing the force as a function of time, we can see how the principal strain (> 5%) criterion grows spatially over time as demonstrated by Figure 7. The free conditions produce a higher injury at each point but similar patterns are developed by both conditions where the injury starts at the exterior (grey matter) of the brain and develops over the interior (white matter) later.

Study 2. Trosseille *et al.* [59]

Experiment Setup

The experimental approach by Trosseille *et al.* was similar to that of Nahum *et al.* Re-pressurized human cadavers were instrumented with skull and intracranial pressure sensors and accelerometers to monitor the effect of impacting the front of the head. Experiment 428-2, where the cadaver was seated in an upright position and impacted with a steering wheel on the face in the anterior-posterior direction (see schematic in Figure 8), was chosen for comparison with the simulation model.

Particular Challenges

Trosseille *et al.* did not provide a sufficient description of the impact conditions, the impactor shape or any impact force measurements. To surmount this, there was no choice but to use the kinematic measurements on the skull as loading input in the simulation. By applying a uniform motion to the skull, we explicitly assumed that the

deformation of the skull and the local differences in acceleration of the head can be neglected, which is an oversimplification because localized stress wave propagation in the viscoelastic brain cannot necessarily be correlated to acceleration data from the relatively stiff skull.

Since discrete experimental data was not available a graphical extraction was used to obtain the acceleration and pressure data from the plots in the report. NRL-HFHM was developed as a neck upward model but the experiments by Trosseille *et al.* work used a full-body PMHS. As a result, free boundary conditions for NRL-HFHM were chosen based on the Nahum *et al.* simulations, where it was observed that these conditions had no significant effect on early pressures when the peak occurs. However, they would likely inaccurately estimate mechanical predictor values at later times of simulation compared to a full body model.

Sensor position concerns and insufficient details on the accuracy in experimental measurement also became a challenge. For example, sensor locations were provided using an anatomical reference frame but the PMHS head size details were not provided, and had to be assumed for comparison with acceleration and pressure data from NRL-HFHM. The accelerometer used in the PMHS did not appear to be of neutral density with respect to the brain, but no details were provided to include the accelerometer as a discrete item in NRL-HFHM for the simulation cases. Therefore, we assumed that the effect of mass of these transducers could be neglected and the acceleration response would be same without the transducer at the measurement location.

Comparison & Analysis

Figure 9 compares the data from the PMHS study of Trosseille *et al.* and the simulation using NRL-HFHM for four regions of the brain – pressure from frontal, parietal, and occipital regions, and acceleration from the occipital region. The experimental and simulation data show mixed agreement.

In the frontal region, after the initial peak pressure, a slight negative pressure is predicted as would be expected due to the negative input acceleration. The experiment shows a secondary effect resulting in a second peak in the pressure profile. This second peak could be the result of movement of the pressure sensor in the tissue, a secondary smaller pressure pulse from skull deformation, or mismatch in boundary conditions between simulation and experimentation. The local deformation, as previously stated, was not accounted for in the simulation because global kinematic profile was applied rather than the force over an area on the head. In the parietal region, a good agreement is not seen. Earlier researchers have often not compared against this experimental pressure when validating their simulations [5] or showed similar predictions to NRL-HFHM [16,57]. This discrepancy is likely the result of the incorrect pressure measurement in the experiment, as we should expect a distinct peak as was seen in the frontal region in this experiment and as was seen in the validation against the Nahum *et al.* experiments. No such peak is seen in Trosseille *et al.* In the occipital region, we see a

good comparison albeit with clearly demonstrated fluctuations in the simulation data noise. The noise from the simulation cannot be compared to the noise from the experiment as no information was provided on filtering or if any was used. Note that the presence of high frequency fluctuations in the simulation correlates with the input acceleration profile applied to the skull indicating that predicted behavior is expected from the simulation. The acceleration response predicted in the brain agrees well with the response of the PMHS. This is, in fact, a more reassuring result in terms of validation because kinematic input was applied to the skull and the output was measured inside the brain. Compared to kinetic input and output—where differences in the sites of application and measurement become moot because the force equilibrium enforcement in the finite element framework overwhelms differences in constitutive descriptions, *i.e.,* what you put in is what you get especially for the primary pulse and near-incompressible materials—this result confirms the choice of the constitutive descriptions with relative merit.

We next use the simulation results to assess the likelihood of injury to a human brain subjected to similar loading conditions. We notice that the frontal pressure of this study is much lower than the frontal pressure measurement in the Nahum *et al.* study due to the lower impact force. As a result, the injury predictions shown in Figure 10 are lower than those shown in the Nahum *et al.* study (Figure 6). Rather than examining the injury pattern as before, we will comment on the challenge in using mechanical injury predictors in an FE simulation. Note that in Figure 10, we have included all non-zero criteria rather than the non-negligible criteria as before, which shows that a small volume of the brain (*e.g.,* 0.2% means 3 cm^3) experiencing injury. This type of data needs to be qualified with an accurate quantification of uncertainty so that a precise confidence bound or limit can be assigned to the predicted injury. This uncertainty quantification will resolve such questions as to whether the predicted 0.2% by volume injury is merely an error to be neglected or an actual risk. However, this task is not trivial and needs to account for uncertainty in geometry due to MRI/CT scan resolutions, uncertainty in material properties, uncertainly in constitutive models, and uncertainty associated with injury predictors among other possible sources of uncertainty.

Study 3. Hardy *et al.* [60,61]

Experiment Setup

Hardy *et al.* conducted impact tests on a number of inverted PMHS head and neck specimens, both with and without helmets. The heads were re-pressurized to minimize the effects of the post mortem state on the specimens. For validating NRL-HFHM, we use experiment number C241, which was the youngest specimen (61 years of age) with a head breadth of 14.5 cm. In particular, we focus on only T5 (offset occipital impact) and T6 (aligned occipital impact) cases which did not use the helmet, and are shown schematically in Figure 11. NRL-HFHM was used with free boundary conditions to

simulate the tests as the torso is not included in the experiment. Head kinematics, coup and counter coup pressure and relative brain motion were measured during the experiments.

Particular Challenges

As with the Trosseille *et al.* study, the experimental set up is not easily replicable in a computational model because enough detail is not provided on the impactor or the impact. A tetrahedral nine-accelerometer array using Endevco 7264C-2kTZ accelerometers was mounted on a nylon pedestal and installed in the maxillary sinus to measure the acceleration in the experiment [61]. Consequently, acceleration measurements on the sinus are used instead of impactor force-time data. As before, the accelerations are applied to the whole head to simulate the impact.

Acceleration data was filtered using a CFC 180 Hz profile as part of the experimental study, which was extracted graphically for use in the computational model. The pressure sensors were mounted in the brain tissue, but their locations were only shown schematically and described as coup and countercoup, and not exactly specified. The pressure data was also filtered using a low pass CFC 1 kHz profile after the experiments. The absence of the raw sensor data added to the challenges in validating the simulation models as the different filters applied on input data (acceleration) and response data (pressure) could not be replicated for the simulation data.

Comparison & Analysis

The comparison between experimental and simulated pressures is shown in Figure 12, which shows acceptable agreement on peak pressure magnitudes and the overall pressure profiles up to 6-7 ms in both coup and countercoup locations for both T5 and T6 cases. Significant differences are noted after this time for each location of either experiment shown in Figure 12, however, as the simulated pressure subsides to near zero much quicker than the experimentally measured pressure. The experimental variations may have been caused by localized damage that increased the pressure in the brain (e.g. significant skull flexure or fracture) during actual experiments that was not captured in the model due to loading method. Nevertheless, this must be viewed in the context of the ambiguities in the actual force applied, location of sensors, and filtering of the data.

Much like the Trosseille *et al.* study, the pressures measured at the coup sites in the experiment are much less than 150 kPa, thus we expect a similar injury volume (<1%) to that in the Trosseille *et al.* study. As with the Trosseille *et al.* comparison (Figure 10), we show all non-zero criteria. The pressures measured are slightly higher than those in the Trosseille *et al.* study, which results in slightly greater injured volumes with higher stress and strain thresholds being predicted as shown in Figure 13. Based on the input loading data, sensor location details and the measured pressures in the two

papers, it is conjectured that there is little difference between the injured volume predictions between the two studies which fall within experimental uncertainty.

Study 4. Yoganandan *et al.* [62]

Experiment Setup

The final experiment considered for this validation is that of Yoganandan *et al.* where a PMHS was impacted on the crown of the head using a hemispherical impactor. The primary objective of this work was to examine skull fracture and the PMHS specimens were chosen to exclude subjects with severe degenerative or bone disease. Consequently, the experimental data serves as a validation of the structural response of the head, and not of the response of the brain to the blunt impact loading. The experimental data from Case 7—impact on an un-embalmed cadaver, a 65-year-old, 95 kg male, with an impact speed of 7.2 m/s—was used for this validation. Impact force was measured using a load cell below the head while displacement was measured from the motion of the piston. The experimental set up is shown schematically in Figure 14. The displacement-time curve was derived from the experimental impact velocity and was used as input to simulate the impact using NRL-HFHM. The displacement curve is omitted in Figure 14 because it is linear as one would expect from a constant velocity. The authors did not specify if PMHS repressurization was used as with the previous three experiment studies.

Particular Challenges

Due to the simplicity of the experiment, few challenges were encountered in developing an equivalent for the simulation. The description of the impactor allowed for exact simulation of the impact. Boundary conditions were specified to be fixed around the internal auditory meatus of the skull. Since the size of the pin used to fix the skull in place was not provided, this pin was assumed to be 12.5 mm in diameter (see Figure 14b).

Comparison & Analysis

Overall NRL-HFHM simulation and the experimental data compare well (Figure 15). The deviation for displacements greater than 5 mm is due to permanent deformation followed by fracture of the skull, which is not captured in the current simulation, as bone damage is not included in the constitutive description. The excellent correlation between simulated and experimental results indicates that the *in-silico* model captures the overall structural response of the head (dominated by the stiff skull) reasonably well.

Due to the location and type of impactor as well as the boundary conditions, we see a much greater injury here than in the previous studies as demonstrated by

Figure 16 a) and b). In the previous studies, the forces applied to the PMHS head were of the same magnitude but the impactor was generally padded and the head was not fixed in the direction of the impact. The combination of these conditions led to fracture in this case and much higher intracranial forces and pressures. Like the study by Nahum *et al.*, we see a severe pressure based injury almost immediately after impact, but observe only a small (<3%) stress and strain based injury prediction. The 1 ms duration over which the data is collected in this study is significantly smaller than the 10 ms of data collection in the experiment of Nahum *et al.*, which dictates the differences between the predicted stress and strain values. In the first study, the 10 ms simulated time and the free boundary condition (and even the fixed boundary condition) at the neck allow the inertial effects to contribute to a higher predicted stress and strain values. In the Yoganandan *et al.* study, the amount of data is over approximately 1 ms and the head is fixed in the direction of the impact. The data limits possible comparison and cannot capture the dynamics of the tissue after the passage of the initial pressure wave and eventual removal of the impactor away from the skull. On the other hand, the fixed boundary condition at the base of the skull would probably result in a much greater transmission of impact energy to the skull and the brain. As illustrated in Figure 16c, the evolution of injured brain volume rapidly saturates to 100% compared to just about 5% in the Nahum case.

Summary and Conclusions

In this work, the challenges in the development and validation of a human head model for the study of traumatic brain injury due to high-rate impact loadings have been presented through the description of the relevant stages for the NRL High-fidelity Head Model (NRL-HFHM). The stages include: i) digital and manual segmentation of MRI scans, ii) meshing (compatible with Abaqus/Explicit), iii) calibration of constitutive models for each component in the brain, and iv) validation against four well-known experimental blunt impact studies. Additionally, the simulations were also used to assess potential injury to a live subject if exposed to the same event based on injury criteria suggested in the literature.

Several specific challenges at each stage of model development and validation have been identified that are universally applicable to any biomechanical model, and especially to a model for analyzing mild to moderate TBI. Suggestions to improve future models and surmount the identified challenges have also been discussed. Here, the overarching roadblocks and potential solutions are summarized:

1. The ubiquitous 1 mm resolution of MRI scans demand that to achieve high fidelity one must intervene manually to account for smaller features, such as the meningeal layers. The lack of gray scale contrast between similar materials can result in their obscurity, which can be ameliorated with the complementary use of CT scans, preferably on the same subject. In both cases, existing CAD based anatomical

descriptions from medical libraries can also be used to complete the anatomical description with fidelity.

2. While meshing with hexahedral elements is desirable due to their superior convergence performance, computational cost can compound with refinement needed to secure high fidelity. Modified quadratic ten-node tetrahedral [41] and hybrid volume-averaged pressure linear tetrahedral [39] elements offer a compromise in computational cost and possible model fidelity. In any case, the use of other element types is unavoidable, *e.g.,* shell elements for arterial walls and meningeal membranes.
3. The specification of contact conditions between various components of the human head is arguably the biggest challenge in accurately simulating dynamic wave propagation in the brain. Presently, simplified tied and sliding contact conditions are used, which do not capture the true boundary conditions associated with the tethering of the brain to the skull through discrete but considerable vascular, arterial, and membranous anchors that are structurally very complex. Available FE contact models are not adequate to represent the interfacial interactions at these boundaries in an aggregated or nodal level. Similarly, the transduction of stress waves through the multi-layered brain-pia-arachnoid-dura-skull complex is an even more challenging conundrum. A simple change in contact conditions and component material behavior in this complex can cause impedance mismatches enough to reverse wave sign and drastically affect pulse magnitude. However, the reality is that modelers must make do with the simplifications until experimental efforts elucidate the functions, mechanisms, and morphologies further. Refs. [46–49] have been identified as studies towards that end.
4. Unless biomechanical testing procedures and standards are enacted and accepted en masse by the community, characterization of head component material response under equivalent loading conditions as those suffered in an actual impact event will, at best, be flawed. However, given that, effort should be put in accruing as much data as possible for a component to ensure that the most suitable constitutive formulation can be chosen and the non-uniqueness in calibration is minimized, provided the accumulated data representing various subjects and testing protocols is found to be procedurally consistent. Several examples using this strategy can be seen in [52].
5. The challenge in validation is the reliance on older data, which was never accrued with model validation in mind. Thus, crucial details on impactors, impact location, sensors, sensor locations, boundary conditions, etc. are found wanting. Similarly, the experimental output being pressure limits the ability to validate. In this context, this should not come as a surprise that a plethora of head models based on different subjects, meshing schemes, boundary and contact conditions, and constitutive formulations have managed to provide acceptable predictions of the experimental pressure profiles. The use of near-incompressible material definition

for the brain and dynamic equilibrium enforcement in the finite element scheme warrants this unanimity. Perhaps, newer efforts will pay attention to the details in describing the experimental set ups as well as providing kinematic output for model validation. In this regard, [47] is a good example.

Acknowledgment

The authors acknowledge Dr. Ross Cotton from Simpleware® for the generation of the finite element meshes. Dr. Thomas O'Shaughnessy from NRL and Dr. Phil Bayly from Washington University are thanked for technical discussions. Dr. Gary Tan is thanked for reviewing the manuscript and providing useful editorial comments.

This work was supported by the Office of Naval Research (ONR) under contract number N001415WX00531 and the Department of Defense (DoD) High Performance Computing Modernization Program (HPCMP) using the Air Force Research Laboratory (AFRL) Major Shared Resource Center (MSRC) under project 416, subproject 231. Partial funding for this project was provided by the Office of Naval Research (ONR) through the Naval Research Laboratory's Basic Research Program. SQ acknowledges the support of the National Science Foundation under the Internal Research & Development Program.

References

[1] Khalil, T. B., Goldsmith, W., and Sackman, J. L., 1974, "Impact on a Model Head-Helmet System," Int. J. Mech. Sci., **16**(9), pp. 609–625.

[2] Ward, C., and Thompson, R., 1975, "The Development of a Detailed Finite Element Brain Model," Stapp Car Crash Conf. Proc., p. SAE Technical Paper 751163.

[3] Dimasi, F., Marcus, J., and Eppinger, R. H., 1993, "3-D (Three-Dimensional) Anatomic Brain Model for Relating Cortical Strains to Automobile Crash Loading," Proc. Int. Tech. Conf. Enhanc. Saf. Veh., **1993**, pp. 916–924.

[4] "Dynamic Response of Human Head to Impact--Ruan et Al 1994.pdf."

[5] Umr, C., Willinger, R., Kang, H. S., Diaw, B., and Umr, C., 1999, "Three-Dimensional Human Head Finite-Element Model Validation against Two Experimental Impacts," Ann. Biomed. Eng., **27**(3), pp. 403–410.

[6] King, A. I., Ruan, J. S., Zhou, C., Hardy, W. N., and Khalil, T. B., 1995, "Recent Advances in Biomechanics of Brain Injury Research: A Review," J. Neurotrauma, **12**(4), pp. 651–658.

[7] National Instute of Health (NIH), National Institute of Mental Health (NIMH), and Research Services Brach (RSB), 1995, "NIH ImageJ, a Public Domain Image Processing and Analysis Program."

[8] National Instute of Health (NIH), and U.S. National Library of Medicine, D. of H. & H. S., 1994, "Visible Human Project."

[9] Kleiven, S., and Von Holst, H., 2002, "Consequences of Head Size Following Trauma to the Human Head," J. Biomech., **35**(2), pp. 153–160.

[10] Horgan, T. J., and Gilchrist, M. D., 2003, "The Creation of Three-Dimensional Finite Element Models for Simulating Head Impact Biomechanics," Int. J. Crashworthiness, **8**(4), pp. 353–366.

[11] Dimasi, F. P., Eppinger, R. H., and Bandak, F. A., 1995, "Computational Analysis of Head Impact Response under Car Crash Loadings," SAE Tech. Pap.

[12] Takhounts, E. G., Eppinger, R. H., Campbell, J. Q., Tannous, R. E., Power, E. D., and Shook, L. S., 2003, "On the Development of the SIMon Finite Element Head Model," Stapp Car Crash J., **47**, pp. 107–33.

[13] Takhounts, E. G., Ridella, S. A., Hasija, V., Tannous, R. E., Campbell, J. Q., Malone, D., Danelson, K., Stitzel, J., Rowson, S., and Duma, S., 2008, "Investigation of Traumatic Brain Injuries Using the next Generation of Simulated Injury Monitor (SIMon) Finite Element Head Model," Stapp Car Crash J., **52**, pp. 1–31.

[14] Zhang, L., Yang, K. H., and King, A. I., 2001, "Comparison of Brain Responses between Frontal and Lateral Impacts by Finite Element Modeling," J. Neurotrauma, **18**(1), pp. 21–30.

[15] Zhang, L., Yang, K. H., and King, A. I., 2004, "A Proposed Injury Threshold for Mild Traumatic Brain Injury," J. Biomech. Eng., **126**(2), pp. 226–236.

[16] Mao, H., Zhang, L., Jiang, B., Genthikatti, V. V., Jin, X., Zhu, F., Makwana, R., Gill,

A., Jandir, G., Singh, A., and Yang, K. H., 2013, “Development of a Finite Element Human Head Model Partially Validated With Thirty Five Experimental Cases,” J. Biomech. Eng., **135**(11), p. 111002.

[17] Moore, D. F., Jérusalem, A., Nyein, M., Noels, L., Jaffee, M. S., and Radovitzky, R. A., 2009, “Computational Biology - Modeling of Primary Blast Effects on the Central Nervous System,” Neuroimage, **47**(SUPPL. 2), pp. T10–T20.

[18] Taylor, P. a, and Ford, C. C., 2009, “Simulation of Blast-Induced Early-Time Intracranial Wave Physics Leading to Traumatic Brain Injury,” J. Biomech. Eng., **131**(6), p. 61007.

[19] El Sayed, T., Mota, A., Fraternali, F., and Ortiz, M., 2008, “A Variational Constitutive Model for Soft Biological Tissues,” J. Biomech., **41**(7), pp. 1458–1466.

[20] El Sayed, T., Mota, A., Fraternali, F., and Ortiz, M., 2008, “Biomechanics of Traumatic Brain Injury,” Comput. Methods Appl. Mech. Eng., **197**(51–52), pp. 4692–4701.

[21] Cloots, R. J. H., Van Dommelen, J. A. W., Kleiven, S., and Geers, M. G. D., 2013, “Multi-Scale Mechanics of Traumatic Brain Injury: Predicting Axonal Strains from Head Loads,” Biomech. Model. Mechanobiol., **12**(1), pp. 137–150.

[22] Erdemir, A., Guess, T. M., Halloran, J., Tadepalli, S. C., and Morrison, T. M., 2012, “Considerations for Reporting Finite Element Analysis Studies in Biomechanics,” J. Biomech., **45**(4), pp. 625–633.

[23] NASA, 1995, “Volume 1, Section 3: Anthropometry and Biomechanics. Man-System Integration Standards.”

[24] Zhang, L., Yang, K. H., and King, A. I., 2001, “Biomechanics of Neurotrauma,” Neurol. Res., **23**(2–3), pp. 144–156.

[25] Deck, C., and Willinger, R., 2008, “Improved Head Injury Criteria Based on Head FE Model,” Int. J. Crashworthiness, **13**(6).

[26] Margulies, S. S., and Thibault, L. E., 1992, “A Proposed Tolerance Criterion for Diffuse Axonal Injury in Man,” J. Biomech., **25**(8).

[27] Kleiven, S., 2007, “Predictors for Traumatic Brain Injuries Evaluated through Accident Reconstructions.,” Stapp Car Crash J., **51**.

[28] Wright, R. M., and Ramesh, K. T., 2012, “An Axonal Strain Injury Criterion for Traumatic Brain Injury,” Biomech. Model. Mechanobiol., **11**(1–2), pp. 245–260.

[29] Kang, H.-S., Willinger, R., Diaw, B. M., and Chinn, B., 1997, “Validation of a 3D Anatomic Human Head Model and Replication of Head Impact in Motorcycle Accident by Finite Element Modeling,” *Stapp Car Crash Conference Proceedings*.

[30] Qidwai, S. M., Kota, N., Leung, A. C., and Bagchi, A., 2013, “Comparison of Mechanical Variable Identifiers of Brain Injury,” *ASME 2013 Summer Bioengineering Conference, SBC 2013*, ASME, Sunriver, OR.

[31] Smith, D. H., Meaney, D. F., and Shull, W. H., 2003, “Diffuse Axonal Injury in Head Trauma,” J. Head Trauma Rehabil., **18**(4), pp. 307–316.

[32] Spaethling, J. M., Geddes-Klein, D. M., Miller, W. J., von Reyn, C. R., Singh, P., Mesfin, M., Bernstein, S. J., and Meaney, D. F., 2007, “Linking Impact to Cellular

and Molecular Sequelae of CNS Injury: Modeling in Vivo Complexity with in Vitro Simplicity," Prog. Brain Res., **161**, pp. 27–39.

[33] Young, P. G., Beresford-West, T. B. H., Coward, S. R. L., Notarberardino, B., Walker, B., and Abdul-Aziz, A., 2008, "An Efficient Approach to Converting Three-Dimensional Image Data into Highly Accurate Computational Models," Philos. Trans. R. Soc. A Math. Phys. Eng. Sci., **366**(1878), pp. 3155–3173.

[34] Cotton, R. T., Pearce, C. W., Young, P. G., Kota, N., Leung, A. C., Bagchi, A., and Qidwai, S. M., 2015, "Development of a Geometrically Accurate and Adaptable Finite Element Head Model for Impact Simulation: The Naval Research Laboratory–Simpleware Head Model," Comput. Methods Biomech. Biomed. Engin., **5842**(May), pp. 1–13.

[35] Wang, G., and Yu, H., 2013, "The Meaning of Interior Tomography," Phys. Med. Biol., **58**(16), pp. 5764–5767.

[36] Wang, G., Kalra, M., Murugan, V., Xi, Y., Gjesteby, L., Getzin, M., Yang, Q., Cong, W., and Vannier, M., 2015, "Vision 20/20: Simultaneous CT-MRI — Next Chapter of Multimodality Imaging," Med. Phys., **42**(10), pp. 5879–5889.

[37] Young, P. G., Tabor, G., Collins, T., Richterova, J., Dejuniat, E., and Beresford-West, T., 2006, "Automating the Generation of 3D Finite Element Models Based on Medical Imaging Data," *Digital Human Modeling for Design and Eng. Conf.*

[38] Dassault Systèmes Simulia Corp., 2016, "Abaqus 2016, Theory, Benchmarks, and Examples Manuals."

[39] Bonet, J., and Burton, A. J., 1998, "A Simple Average Nodal Pressure Tetrahedral Element for Incompressible and Nearly Incompressible Dynamic Explicit Applications," Commun. Numer. Methods Eng., **14**(March 1997), pp. 437–449.

[40] Danielson, K. T., 2014, "Fifteen Node Tetrahedral Elements for Explicit Methods in Nonlinear Solid Dynamics," Comput. Methods Appl. Mech. Eng., **272**, pp. 160–180.

[41] Reddy, J. N., 1993, *An Introduction to the Finite Element Method*, McGraw-Hill New York.

[42] Chafi, M. S., Karami, G., and Ziejewski, M., 2010, "Biomechanical Assessment of Brain Dynamic Responses due to Blast Pressure Waves," Ann. Biomed. Eng., **38**(2), pp. 490–504.

[43] Al-Bsharat, A. S., Hardy, W. N., Yang, K. H., Khalil, T. B., Tashman, S., and King, A. I., 1999, "Brain/skull Relative Displacement Magnitude due to Blunt Head Impact: New Experimental Data and Model," *Stapp Car Crash Conference Proceedings*, SAE, San Diego, CA, USA, pp. 321–332.

[44] Hrapko, M., Van Dommelen, J. A. W., Peters, G. W. M., and Wismans, J. S. H. M., 2009, "On the Consequences of Non Linear Constitutive Modelling of Brain Tissue for Injury Prediction with Numerical Head Models," Int. J. Crashworthiness, **14**(3), pp. 245–257.

[45] Feng, Y., Abney, T. M., Okamoto, R. J., Pless, R. B., Genin, G. M., and Bayly, P. V, 2010, "Relative Brain Displacement and Deformation during Constrained Mild

Frontal Head Impact," J. R. Soc. Interface, **7**(53), pp. 1677–1688.
[46] Saboori, P., and Sadegh, A., 2015, "Histology and Morphology of the Brain Subarachnoid Trabeculae.," Anat. Res. Int., **2015**, p. 279814.
[47] Badachhape, A. A., Okamoto, R. J., Durham, R. S., Efron, B. D., Nadell, S. J., Johnson, C. L., and Bayly, P. V., 2017, "The Relationship of Three-Dimensional Human Skull Motion to Brain Tissue Deformation in Magnetic Resonance Elastography Studies," J. Biomech. Eng., **139**(5), p. 51002.
[48] Scott, G. G., and Coats, B., 2015, "Microstructural Characterization of the Pia-Arachnoid Complex Using Optical Coherence Tomography," IEEE Trans. Med. Imaging, **34**(7), pp. 1452–1459.
[49] Feng, Y., Abney, T. M., Okamoto, R. J., Pless, R. B., Genin, G. M., and Bayly, P. V, 2010, "Relative Brain Displacement and Deformation during Constrained Mild Frontal Head Impact.," J. R. Soc. Interface, **7**(53), pp. 1677–88.
[50] Bower, A. F., 2009, *Applied Mechanics of Solids*, CRC press.
[51] Veryst Engineering, 2016, "MCalibration."
[52] Brewick, P., Saunders, R., and Bagchi, A., 2017, "Biomechanical Modeling of the Human Head," Def. Tech. Inf. Cent., (NRL/FR/6350--17-10,304).
[53] Ogden, R. W., Saccomandi, G., and Sgura, I., 2004, "Fitting Hyperelastic Models to Experimental Data," Comput. Mech., **34**(6), pp. 484–502.
[54] Romanov, K. I., 2001, "The Drucker Stability of a Material," J. Appl. Math. Mech., **65**(1), pp. 155–162.
[55] Anderson, A. E., Ellis, B. J., and Weiss, J. A., 2007, "Verification, Validation and Sensitivity Studies in Computational Biomechanics," Comput. Methods Biomech. Biomed. Engin., **10**(3), pp. 171–184.
[56] Henninger, H. B., Reese, S. P., Anderson, a E., and Weiss, J. a, 2010, "Validation of Computational Models in Biomechanics.," Proc. Inst. Mech. Eng. H., **224**(7), pp. 801–812.
[57] Deck, C., and Willinger, R., 2009, "The Current State of the Human Head Finite Element Modelling," Int. J. Veh. Saf., **4**(2), pp. 85–112.
[58] Nahum, A. M., Smith, R., Raasch, F., and Ward, C. C., 1977, "Intracranial Pressure Dynamics during Head Impact," Stapp Car Crash Conf. Proc., pp. 615–636.
[59] Trosseille, X., Tarriere, C., and Lavaste, F., 1992, "Development of a FEM of the Human Head according to a Specific Test Protocol," 30th Stapp Car Crash Conf. Proc., pp. 235–253.
[60] Hardy, W. N., Foster, C. D., Mason, M. J., Yang, K. H., King, a I., and Tashman, S., 2001, "Investigation of Head Injury Mechanisms Using Neutral Density Technology and High-Speed Biplanar X-Ray.," Stapp Car Crash J., **45**(November), pp. 337–368.
[61] 2007, "A Study of the Response of the Human Cadaver Head to Impact."
[62] Yoganandan, N., Pintar, F. A., Sances Jr., A., Walsh, P. R., Ewing, C. L., Thomas, D. J., and Snyder, R. G., 1995, "Biomechanics of Skull Fracture," J. Neurotrauma, **12**(4), pp. 659–668.

[63] Hrapko, M., Van Dommelen, J. A. W. A. W., Peters, G. W. M. W. M., and Wismans, J. S. H. M. S. H. M., 2008, "The Influence of Test Conditions on Characterization of the Mechanical Properties of Brain Tissue," ournal Biomech. Eng., **130**(June 2008), pp. 31003–1.

[64] Prange, M. T., and Margulies, S. S., 2002, "Regional, Directional, and Age-Dependent Properties of the Brain Undergoing Large Deformation," J. Biomech. Eng., **124**(2), p. 244.

[65] Gur, R. C., Mozley, P. D., Resnick, S. M., Gottlieb, G. L., Kohn, M., Zimmerman, R., Herman, G., Atlas, S., Grossman, R., and Berretta, D., 1991, "Gender Differences in Age Effect on Brain Atrophy Measured by Magnetic Resonance Imaging.," Proc. Natl. Acad. Sci. U. S. A., **88**(7), pp. 2845–9.

[66] Gefen, A., Gefen, N., Zhu, Q., Raghupathi, R., and Margulies, S. S., 2003, "Age-Dependent Changes in Material Properties of the Brain and Braincase of the Rat," J. Neurotrauma, **20**(11), pp. 1163–1177.

[67] Salimi Jazi, M., Rezaei, A., Azarmi, F., Ziejewski, M., and Karami, G., 2016, "Computational Biomechanics of Human Brain with and without the Inclusion of the Body under Different Blast Orientation," Comput. Methods Biomech. Biomed. Engin., **19**(9), pp. 1019–1031.

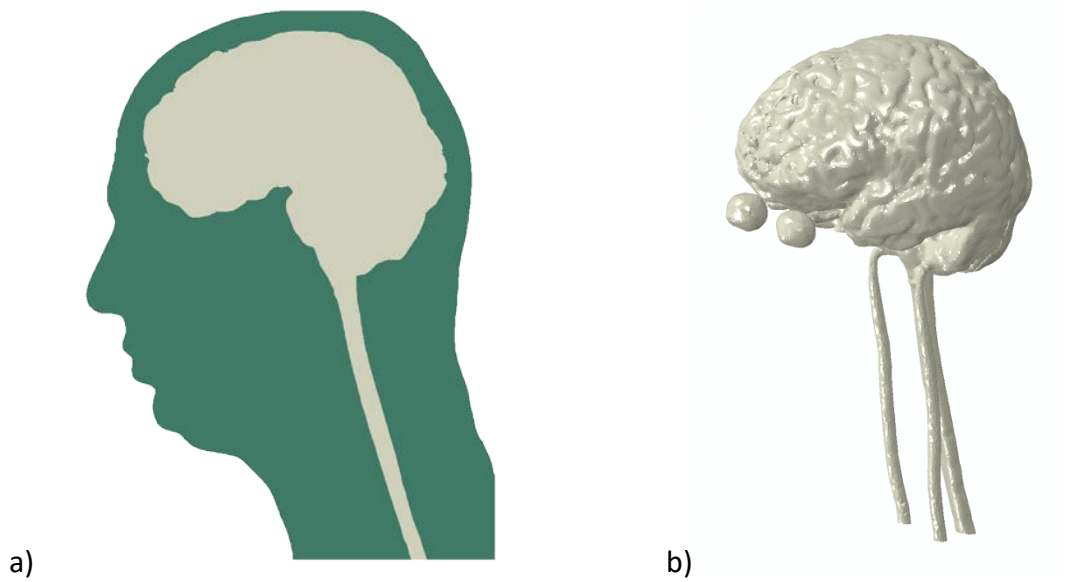

Figure 1: Distribution of linear and quadratic elements in the head model. The darker color in a) represents the region with linear elements, and the lighter color in a) and b) represents the regions with quadratic elements. The region containing brain, CSF, eyes, etc., shown on the right b), is fully composed of quadratic elements.

Figure 2: Skull partitioning for assigning material orientation. Each color patch represents a one of 1000 regions with unique orientation assignment.

a)

b)

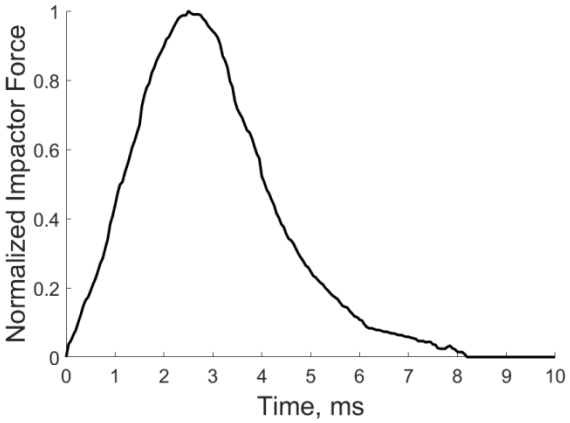

Figure 3: Experimental setup of Nahum *et al.*, a) Representative impactor shown impacting NRL-HFHM at a 45 degree incline, b) Normalized impactor force over time.

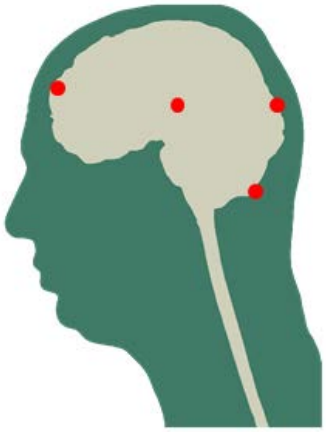

Figure 4: Locations of pressure measurement in NRL-HFHM for the experiment of Nahum *et al.* Note: the sensor in the middle of the brain appears as such because of the 2D nature of the graphic.

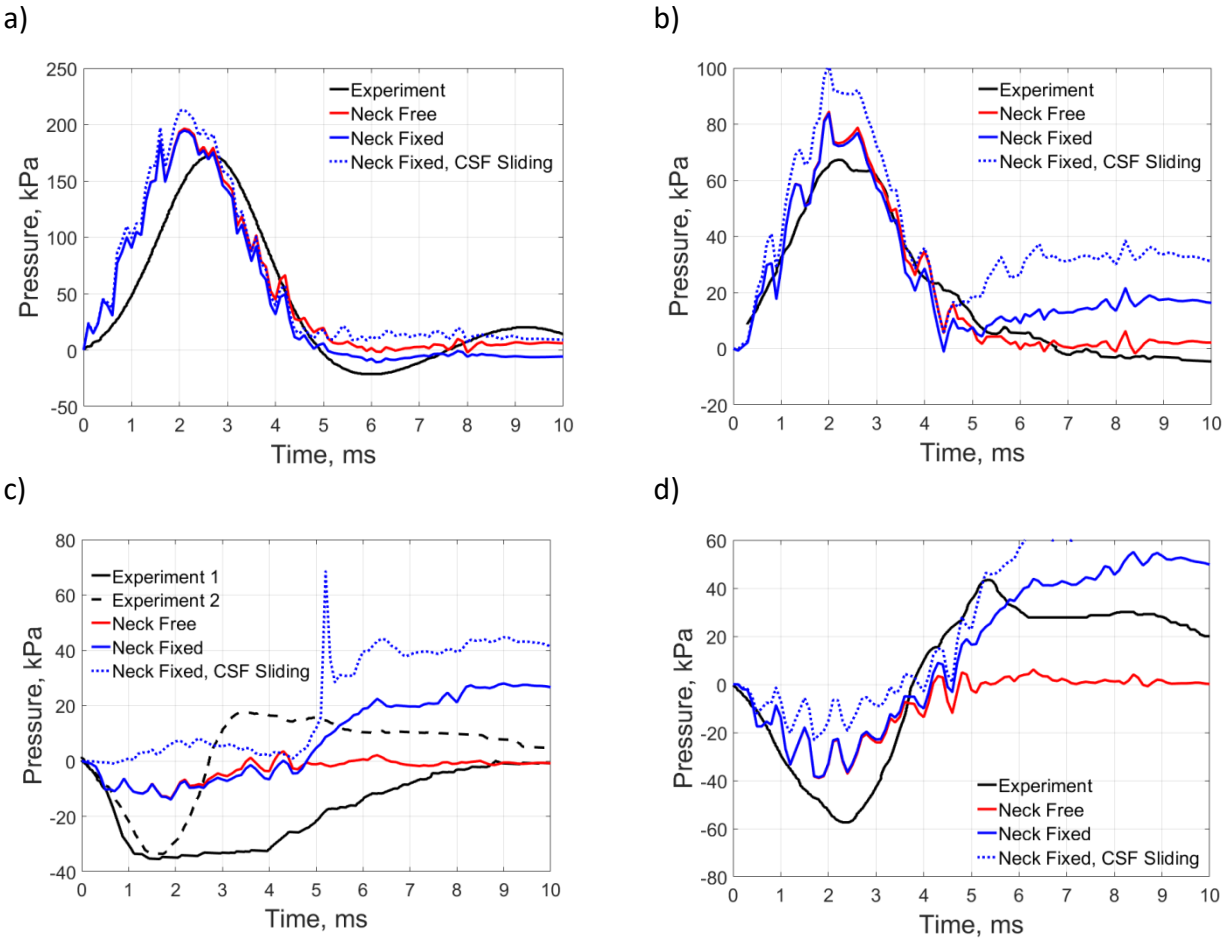

Figure 5: Comparison between simulation and experiments. Intracranial pressures in a) frontal, b) parietal, c) occipital, and d) posterior regions.

a)

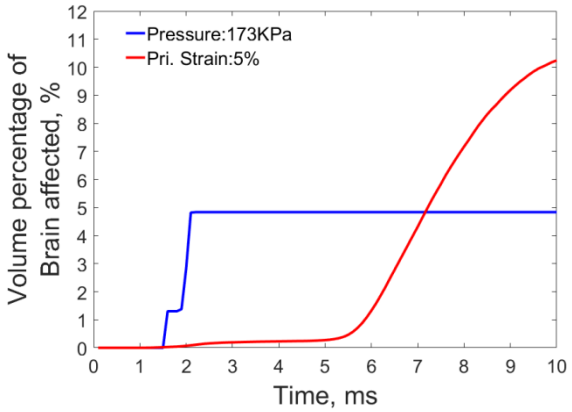

b)

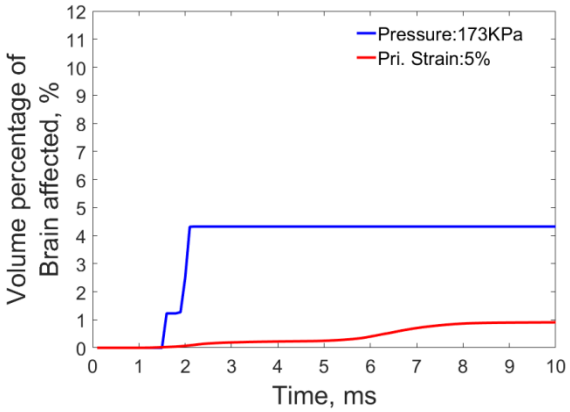

Figure 6: Temporal injury volume predictions based on the metrics of Table 3 using a) free boundary conditions and b) fixed boundary conditions.

a) b)

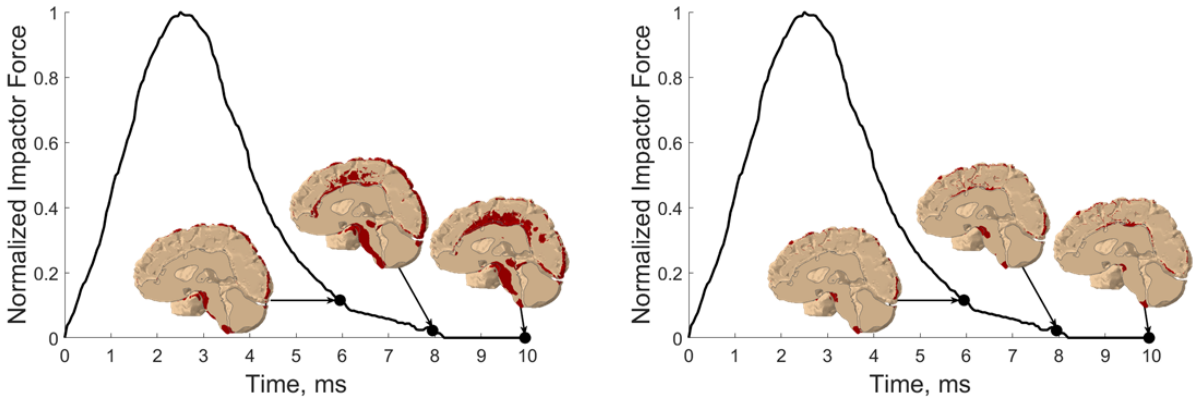

Figure 7: Spatial brain injury using the 5% principal strain criteria at various time points of loading using a) free and b) fixed boundary conditions. The brain is sliced along the median sagittal plane and only the right hemisphere is shown. Injured regions indicated by dark color.

a)

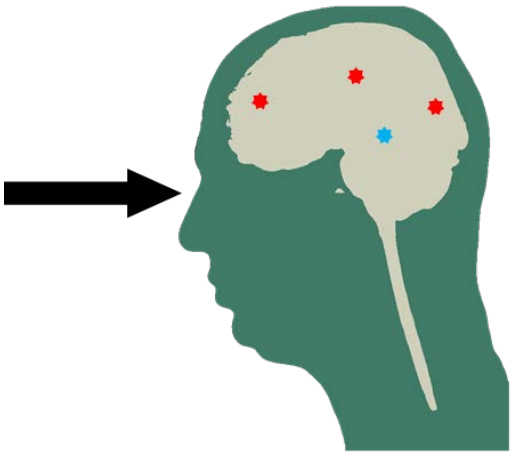

b)

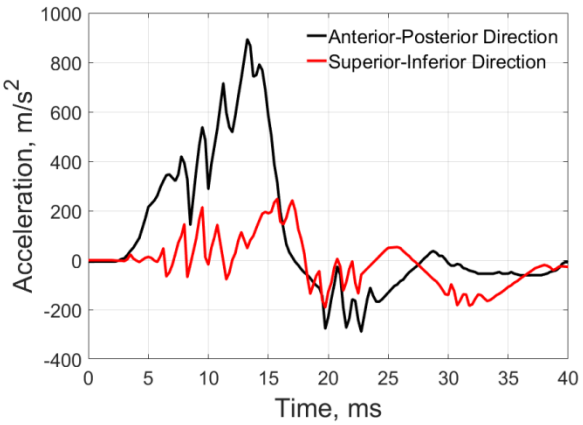

Figure 8: a) Schematic of Trosseile's experiments and locations of measurement. The arrow indicates the direction of impact of steering wheel on to the PMHS. The locations marked in red show the approximate pressure transducer locations while the blue shows the approximate accelerometer location. b) The skull acceleration measurements from experimental data used as the model input.

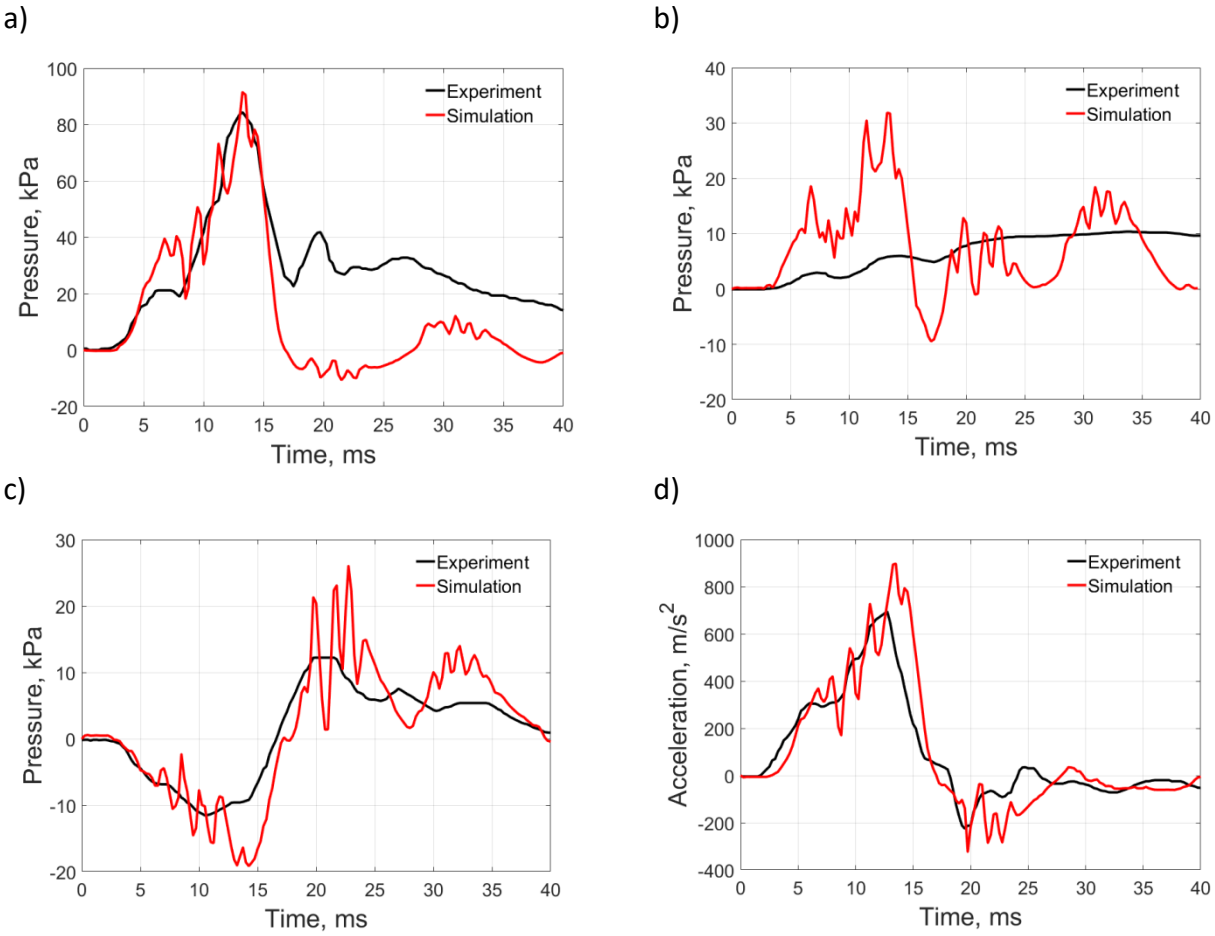

Figure 9: Comparison between experiments and simulation: intracranial pressures in a) frontal, b) parietal, and c) occipital regions; and d) intracranial acceleration in white matter of the occipital lobe.

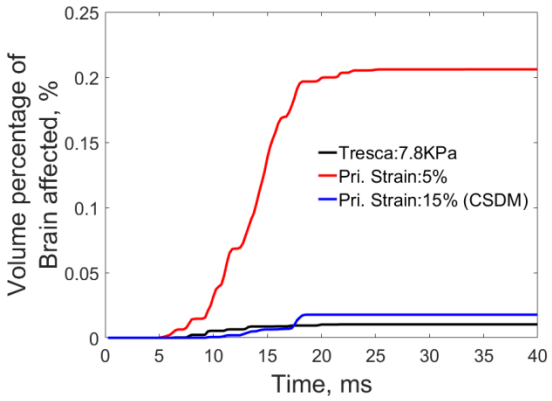

Figure 10: Temporal injury volume predictions based on the metrics of Table 3 using three mechanical injury predictors for the experiment of Trosseille *et al.*

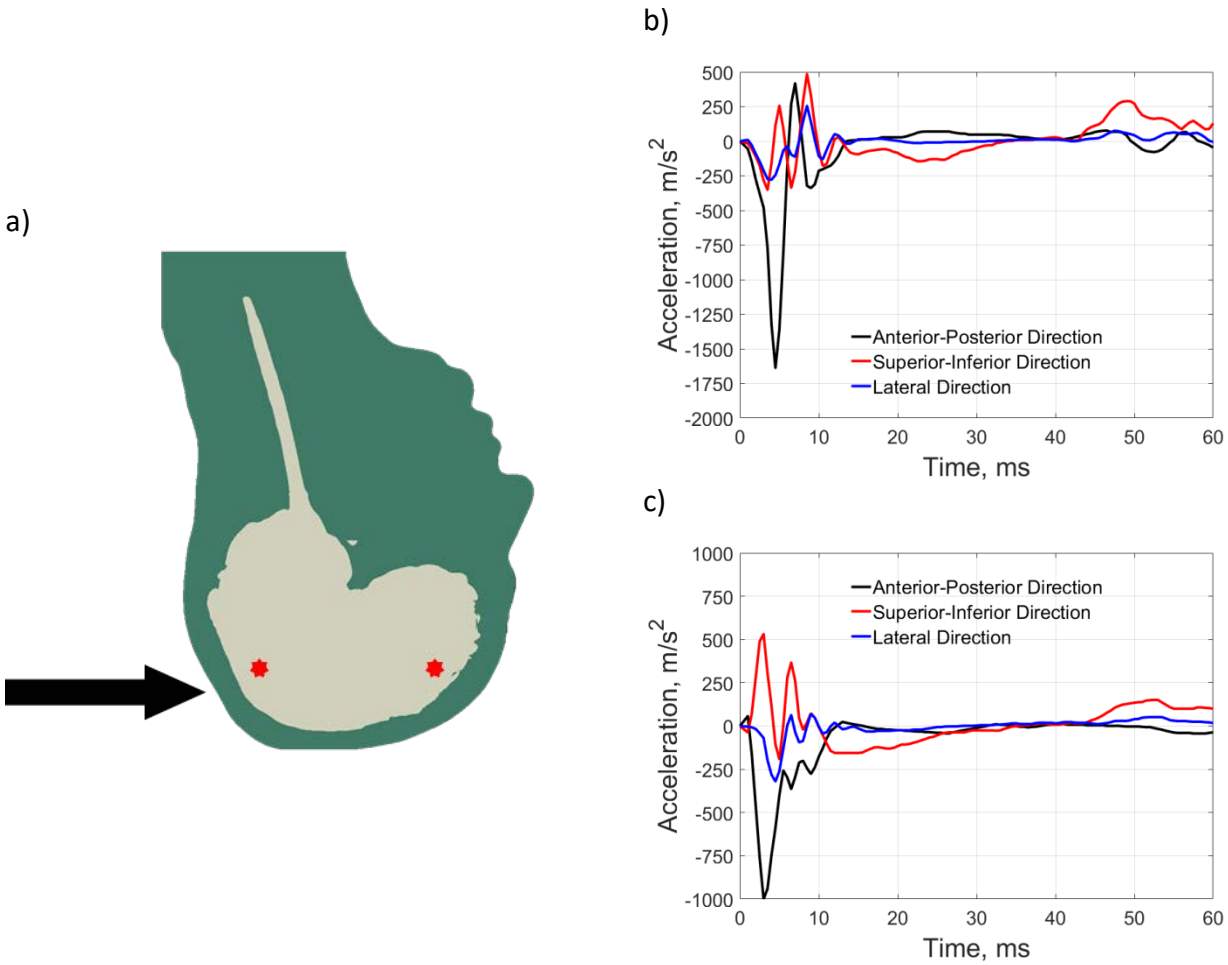

Figure 11: a) Schematic of experiment C241 casesT5 and T6. The arrow indicates the direction of impact. The locations of intracranial pressure measurements are shown in red. The coup location is nearest the impact site and the countercoup furthest. b) Acceleration inputs for the T5 experiment and c) acceleration inputs for the T6 experiment.

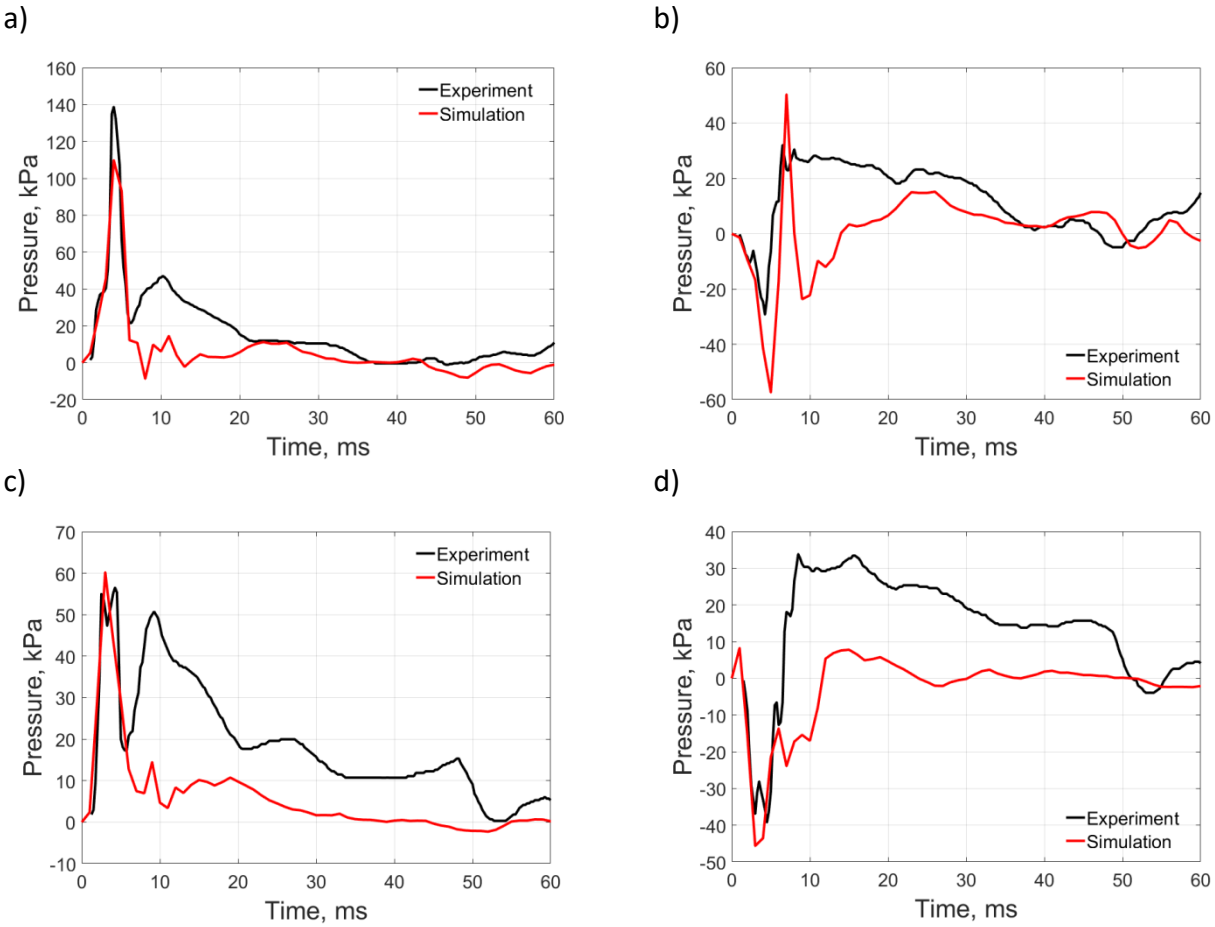

Figure 12: Comparison between simulation and C241 experiments. Comparison of intracranial pressures in a) T5 coup, b) T5 countercoup, c) T6 coup, and d) T6 countercoup regions.

a) b)

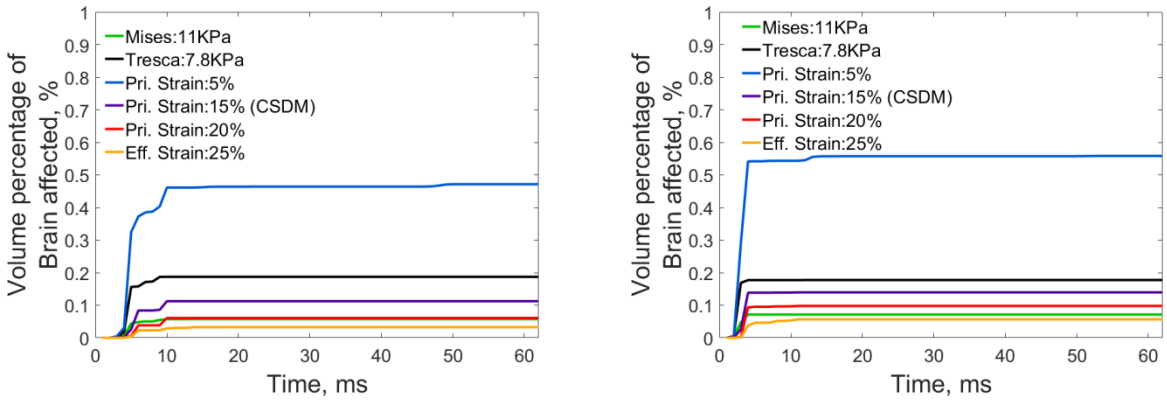

Figure 13: Temporal injury volume predictions based on the metrics of Table 3 using six mechanical injury predictors for the experiment of Hardy *et al.* for simulations of the a) T5 case and b) T6 case.

a) b)

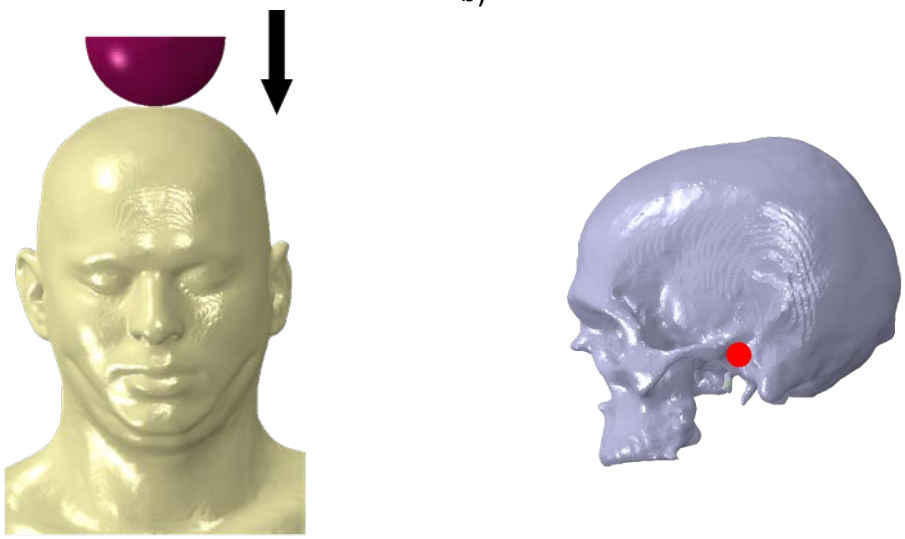

Figure 14: Schematic of case 7 in Yoganandan *et al.* experiment showing a) impact geometry with the hemispherical anvil and the direction of impact, b) Side view of the skull with red spot denoting the fixed region around the internal auditory meatus on both sides of the skull.

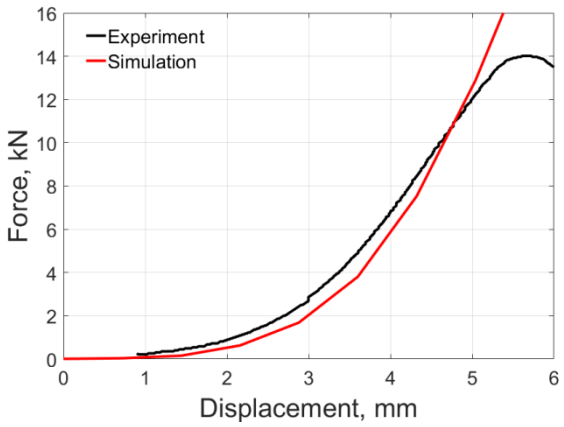

Figure 15: Comparison of force vs displacement characteristics between NRL-HFHM simulation and experimental data from Yoganandan *et al.*

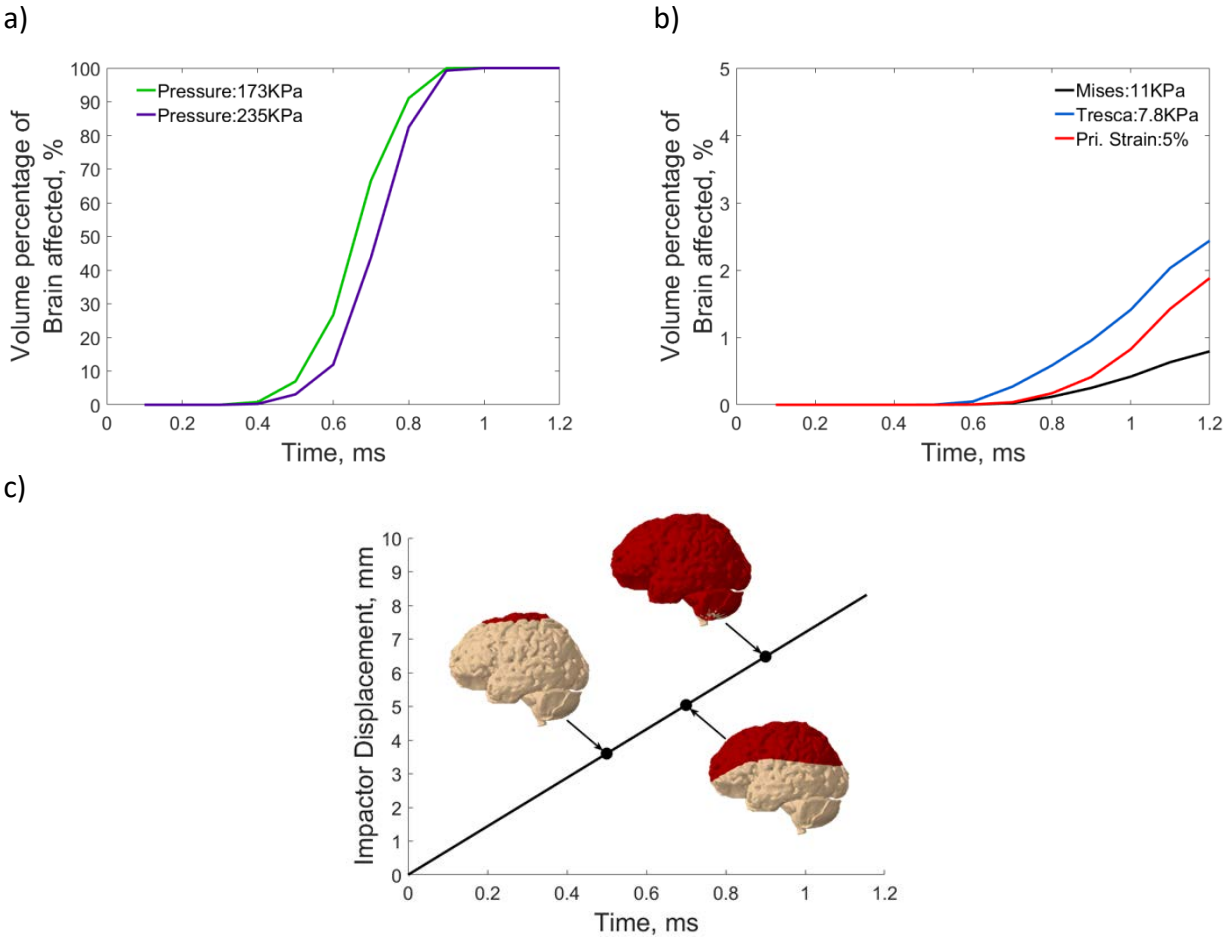

Figure 16: a) Temporal injury for two pressure metrics given in Table 3. b) Temporal injury for three most significant stress and strain metrics given in Table 3. c) Displacement versus time of the impactor with 235 kPa pressure injury volume in the brain shown in dark color.

Table 1: NRL-HFHM anatomical structures and their corresponding constitutive model functional forms

Component	Constitutive Model Functional Form
Sinus - Frontal	Equation of State (Ideal Gas Law)
Sinus - Maxillary	
Airway	
Cerebrospinal Fluid (CSF)	Hyperelastic (neo-Hookean)
Ventricles - Lateral	
Ventricles - Third	
Ventricles - Fourth	
Ventricles - Aqueduct of Sylvius	
Ventricles - Foramen of Monro	
Venous Sinuses and Bridging Veins	
Eyes (Vitreous)	Hyperelastic (neo-Hookean)
Venous Sinus and Bridging Vein Walls (Shell Section)	Anisotropic Hyperelastic (Holzapfel)
Pia Mater (Shell Section)	Hyperelastic (Ogden)
Dura Mater (Shell Section)	Hyperelastic (Ogden)
Falx Cerebri	Hyperelastic (Ogden)
Tentorium Cerebella	Hyperelastic (Ogden)
Sclera\Cornea (Shell Section)	Hyperelastic (Ogden)
Intervertebral Discs	Hyperelastic (Mooney-Rivlin)
Skull - Cortical	Transversely Isotropic Viscoelastic (Prony Series)
Skull - Cancellous	Transversely Isotropic Viscoelastic (Prony Series)
Mandible	Transversely Isotropic Viscoelastic (Prony Series)
Vertebrae	Viscoelastic (Prony Series)
Cerebrum - Grey Matter	Hyper-viscoelastic (Ogden, Prony series)
Cerebellum - Grey Matter	
Cerebrum - White Matter	Hyper-viscoelastic (Ogden, Prony series)
Cerebellum - White Matter	
Brain Stem - Medulla	
Brain Stem - Midbrain	
Brain Stem - Pons	
Spinal Cord	
Optic Nerves	
Skin	Hyperelastic (Ogden)
Muscles	Hyperelastic (Ogden)
Soft Tissue (Adipose)	Hyperelastic (Ogden)

[‡]Grouped materials share the same constitutive model parameters due to similarities in the material.

Table 2: FE model element and node count

Description	**Count**
Total Elements	4613208
Linear Tetrahedral	2994575
Quadratic Tetrahedral	1489549
Linear Triangular	129084
Nodes	2987979
Degrees of Freedom	13589313

Table 3: Biomechanical thresholds of traumatic brain injury suggested by various authors, as indicated authors

Metric	Limit	Injury	Source
Pressure (kPa)	173	Mild TBI	[15]
	235	Severe TBI	
	-100	50% probability of Concussion (DDM[a])	[12]
Effective (von Mises) Stress (kPa)	11	Severe TBI	[29]
	26	50% probability of Mild DAI[b]	[25]
	33	50% Severe DAI	
Shear (Tresca) Stress (kPa)	7.8	50% probability of Mild TBI	[15]
Maximum Principal Strain (%)	5	Moderate DAI	[26]
	15	50% probability of DAI (CSDM[c])	[12]
	18	DAI	[28]
	20	50% probability of Mild TBI	[15]
	21	50% probability of Mild DAI	[27]
	26	50% probability of Mild DAI	
Effective (von Mises) Strain (%)	25	50% probability of Mild DAI	[25]
	35	50% probability of Severe DAI	

[a]DDM: Dilatational Damage Measure

[b]DAI: Diffuse Axonal Injury

[c]CSDM: Cumulative Strain Damage Measure